THE JOURNAL OF PHYSICAL CHEMISTRY LETTERS
A JOURNAL OF THE AMERICAN CHEMICAL SOCIETY

pubs.acs.org/JPCL

Letter

A Hybrid Quantum-Classical Algorithm for Multichannel Quantum Scattering of Atoms and Molecules

Xiaodong Xing, Alejandro Gomez Cadavid, Artur F. Izmaylov, and Timur V. Tscherbul*

Cite This: J. Phys. Chem. Lett. 2023, 14, 6224−6233

Read Online

ACCESS | Metrics & More | Article Recommendations | Supporting Information

ABSTRACT: We propose a hybrid quantum-classical algorithm for solving the time-independent Schrödinger equation for atomic and molecular collisions. The algorithm is based on the *S*-matrix version of the Kohn variational principle, which computes the fundamental scattering *S*-matrix by inverting the Hamiltonian matrix expressed in the basis of square-integrable functions. The computational bottleneck of the classical algorithm—symmetric matrix inversion—is addressed here using the variational quantum linear solver (VQLS), a recently developed noisy intermediate-scale quantum (NISQ) algorithm for solving systems of linear equations. We apply our algorithm to single- and multichannel quantum scattering problems, obtaining accurate vibrational relaxation probabilities in collinear atom−molecule collisions. We also show how the algorithm could be scaled up to simulate collisions of large polyatomic molecules. Our results demonstrate that it is possible to calculate scattering cross sections and rates for complex molecular collisions on NISQ quantum processors, opening up the possibility of scalable digital quantum computation of gas-phase bimolecular collisions and reactions of relevance to astrochemistry and ultracold chemistry.

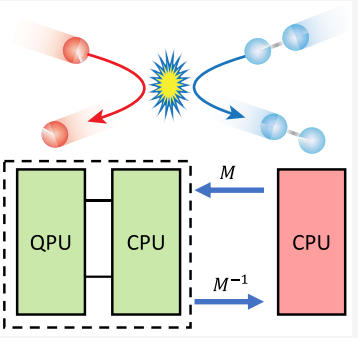

The development of novel algorithms for the digital[1,2] and analog[2,3] quantum simulation of molecular structure and dynamics is a rapidly expanding field of research spanning a wide array of topics, including electronic structure,[2,4−6] vibrational structure and spectroscopy,[2,4−6] and excitonic energy transfer in model biological systems.[7,8] Quantum computers rely on the concepts of quantum superposition and entanglement to process information in more efficient (and in many cases, exponentially more efficient) ways compared to classical computers.[9] Quantum phase estimation (QPE)[10] is the foremost algorithm for solving the Schrödinger equation on fault-tolerant quantum computers.[11,12] While QPE can provide an exponential speedup over classical algorithms, current hardware limitations have prevented its widespread use. More promising for current applications are hybrid quantum algorithms, such as the variational quantum eigensolver (VQE),[13−15] which combines classical and quantum computation to take full advantage of today's limited noisy intermediate-scale quantum (NISQ) resources.[16]

The VQE algorithm consists of four steps[13−15] and begins with the preparation of a trial quantum state (or ansatz) $|\psi(\theta_i)\rangle$, followed by the calculation of the expectation value $\langle\hat{O}\rangle(\theta_i) = \langle\psi(\theta_i)|\hat{O}|\psi(\theta_i)\rangle$ of a quantum observable $\hat{O}$ over the trial state. The optimal values of the variational parameters θ_i are then found using a classical optimization algorithm, and the entire procedure is repeated until convergence of the expectation value. The VQE has been successfully applied to the electronic structure problem[1,2] and to the calculation of molecular vibrational levels,[17] dynamics,[18] and spectra.[19] An alternate approach is based on mapping the vibrational eigenvalue problem onto a quadratic unconstrained binary optimization problem, which could be solved efficiently on quantum annealers.[20,21] The resulting quantum annealer eigensolver was used to obtain the vibrational energy levels of ozone[21] and excited electronic states of NH_3.[22] Efficient quantum circuits have been proposed for VQE calculations of rovibrational energy levels in a discrete variable representation basis.[23]

Quantum scattering phenomena play a fundamental role in physical and theoretical chemistry, being at the heart of gas-phase chemical reaction mechanisms,[24−26] astrochemistry,[27,28] combustion simulations,[29,30] mode-selective chemistry,[31,32] and atmospheric chemistry.[33] In addition, molecular scattering experiments, particularly those performed at low and ultralow temperatures, provide the most detailed information about intermolecular interactions.[34−37] Molecular collisions and chemical reactions at ultralow temperatures determine the stability of ultracold molecular gases, with "good" (elastic) collisions leading to desirable thermalization and "bad" (inelastic) collisions responsible for undesirable trap losses, which limits the stability of trapped molecules.[38−41] A detailed understanding of the quantum dynamics of binary collisions

Received: April 11, 2023
Accepted: June 15, 2023

https://doi.org/10.1021/acs.jpclett.3c00985
J. Phys. Chem. Lett. 2023, 14, 6224−6233

and chemical reactions in ultracold environments may lead to novel ways to control them using, e.g., external electromagnetic fields[38−41] and/or quantum interference effects.[42,43]

To model quantum scattering phenomena, one can use either time-independent or time-dependent (wavepacket) approaches.[24,26,44] Numerically exact quantum scattering simulations, in which the time-independent Schrödinger equation is solved directly via, e.g., coupled-channel methods or basis set expansion techniques,[24−26] are the "gold standard" of chemical physics, similar to the full configuration interaction or high-order coupled-cluster methods in quantum chemistry. When such simulations are performed on classical computers, their computational complexity scales exponentially with the number of molecular degrees of freedom. As such, rigorous calculations are presently limited to systems containing a few atoms.[26]

To address the curse of dimensionality problem in quantum scattering simulations, QPE-based quantum algorithms have been developed for chemical reactions,[45,46] atomic and molecular resonances,[47] and nuclear scattering.[48,49] While these algorithms achieve exponential speedup over their classical counterparts, they are designed for fault-tolerant quantum computers, rather than NISQ devices.[17] Very recently, a hybrid VQE-based quantum algorithm has been proposed for solving the real-time chemical dynamics at low energies.[50] Yet, to our knowledge, no general-purpose quantum algorithm exists for solving the time-independent quantum scattering problem for atoms and molecules on NISQ processors.

Here, we propose and implement such an algorithm based on the S-matrix version of the Kohn variational principle (KVP).[51,52] Our quantum KVP (Q-KVP) algorithm is conceptually simple and has the ability to handle a wide range of elastic, inelastic, and reactive scattering problems on an equal footing using square-integrable (L^2) basis set expansions. The fundamental scattering S-matrix, which encodes all scattering observables, is computed in the KVP using only matrix multiplications and inversions. The most computationally intensive step of the algorithm involves the inversion of a real symmetric Hamiltonian matrix in the basis of real-valued L^2 basis functions. In the Q-KVP algorithm, the inversion problem is solved using the variational quantum linear solver (VQLS), a recently developed NISQ variational algorithm.[53] We illustrate the Q-KVP algorithm by applying it to nontrivial single- and multichannel quantum scattering problems. We finally demonstrate how the Q-KVP algorithm can be scaled up to larger molecular collision systems, which are currently beyond the capabilities of classical computers. Reaching quantum advantage would be a long-term goal, given the maturity of the field of time-independent quantum scattering and the existence of efficient classical algorithms.[24] Our intention here is rather to propose an algorithm that could potentially compete with the classical algorithms. For completeness, we also discuss the issues that can affect the Q-KVP algorithm as one gets close to realizing quantum advantage, such as dealing with very large Hamiltonian matrices.

The key quantity in quantum scattering theory is the multichannel S-matrix with elements $S_{n_f n_i}$, which encode the transition amplitudes between the initial and final channels n_i and n_f. In the framework of the KVP, the S-matrix element is obtained by extremizing the expression[54]

$$S_{n_f n_i}(c_{lm,n}) = \mathrm{ext}[c_{1n_f n_i} + i\langle\tilde{\psi}_{n_f}|\hat{H} - E|\tilde{\psi}_{n_i}\rangle] \tag{1}$$

with respect to the parameters $\{c_{l\,m,n}\}$ of the trial wave functions for the initial and final scattering channels

$$\tilde{\psi}_{n_i}(R, \mathbf{r}) = -u_{0n_i}(R)\phi_{n_i}(\mathbf{r}) + \sum_n c_{1n,n_i}u_{1n}(R)\phi_n(\mathbf{r}) + \sum_{l=2}^{N_l}\sum_{n=1}^{N} c_{ln,n_i}u_{ln}(R)\phi_n(\mathbf{r})$$

$$\tilde{\psi}_{n_f}(R, \mathbf{r}) = -u_{0n_f}(R)\phi_{n_f}(\mathbf{r}) + \sum_n c_{1n,n_f}u_{1n}(R)\phi_n(\mathbf{r}) + \sum_{l=2}^{N_l}\sum_{n=1}^{N} c_{ln,n_f}u_{ln}(R)\phi_n(\mathbf{r}), \tag{2}$$

where $\hat{H}$ is the Hamiltonian of the system (see below), E is the total energy, R is the scattering or reaction coordinate, $\mathbf{r}$ are the internal coordinates of the colliding molecules (such as their vibrational and rotational modes), and $\phi_n(\mathbf{r})$ is an internal wave function. The L^2 basis functions $u_{ln}(R)$, l = 2, 3, ..., and N_l describe the collision complex at short R, and thus $u_{ln}(R) \to 0$ as $R \to \infty$. The total number of scattering channels N includes both open (energetically allowed) and closed (energetically forbidden) channels.

At large R, the last terms on the right-hand side of eq 2 vanish, but the continuum basis functions $u_{0n}(R)$ and $u_{1n}(R) = u_{0n}^*(R)$ do not. We parametrize these functions as[54] (in atomic units, where $\hbar = 1$)

$$u_{0n}(R) = f(R)e^{-ik_nR}v_n^{-1/2},$$
$$u_l(R) = F_lR^{(l-1)}e^{-\gamma R}\ (l = 2, 3, \ldots, N_l), \tag{3}$$

where $k_n = \sqrt{2\mu(E - E_n)}$ is the asymptotic wavenumber in channel n with asymptotic energy E_n, $v_n = k_n/\mu$ is the asymptotic velocity, and μ is the reduced mass for the collision.

Equation 3 ensures that our trial wave functions (2) behave properly in the limit $R \to \infty$, as linear combinations of incoming and outgoing waves (for open channels). The purpose of the cutoff function $f(R) = 1 - e^{-\gamma R}$ in the first line of eq 3 is to regularize the continuum basis functions $u_{0n}(R)$ and $u_{1n}(R) = u_{0n}^*(R)$ at the origin, i.e., to ensure that $u_{0n}(R = 0) = 0$. In eq 3, $\gamma > 0$ is a parameter for the bound-state basis functions $u_{ln}(R)$ with $l \geq 2$ and F_l is a normalization factor. We note that the functions $u_{ln}(R)$ are not necessarily orthogonal, i.e., $\langle u_{ln} \mid u_{l'n}\rangle \neq \delta_{ll'}$ ($l, l' \geq 2$).

By extremizing the expression in eq 1 with respect to the variational parameters of the trial wave function (2), $\frac{\partial}{\partial c_l}[c_{1n_2n_1} + i\langle\tilde{\psi}_{n_2}|\hat{H} - E|\tilde{\psi}_{n_1}\rangle] = 0$, and applying the Löwdin-Feshbach projection technique to separate the matrix operations involving the real and complex matrix elements, we obtain the S-matrix as[52]

$$\mathbf{S} = i(\mathbf{B} - \mathbf{C}^T\mathbf{B}^{*-1}\mathbf{C}), \tag{4}$$

where $\mathbf{S}$, $\mathbf{B}$, and $\mathbf{C}$ are square matrices in the channel index n

$$\mathbf{B} = \mathbf{M}_{0,0} - \mathbf{M}_0^T\mathbf{M}^{-1}\mathbf{M}_0$$
$$\mathbf{C} = \mathbf{M}_{1,0} - \mathbf{M}_0^{*T}\mathbf{M}^{-1}\mathbf{M}_0. \tag{5}$$

Here, $\mathbf{M}_{0,0}$ and $\mathbf{M}_{1,0}$ have the dimensions $N_o \times N_o$, where N_o is the number of open channels (those, for which $k_n^2 > 0$). These

https://doi.org/10.1021/acs.jpclett.3c00985
J. Phys. Chem. Lett. 2023, 14, 6224−6233

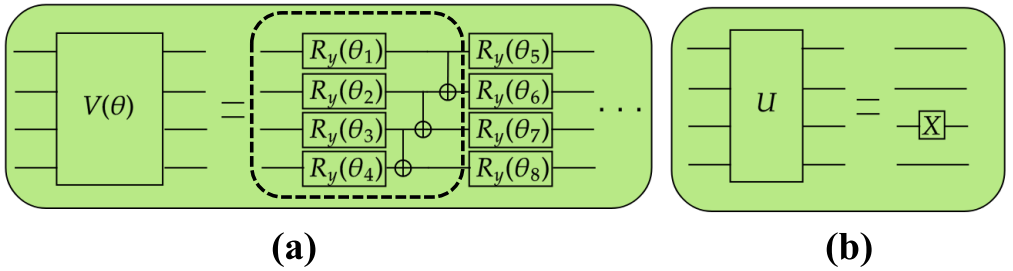

Figure 1. Quantum circuits. (a) The hardware efficient ansatz $V(\theta)$ consists of alternating layers of single-qubit rotations $R_y(\theta_n)$ and controlled-NOT gates.[9] A single repeatable layer is encircled by a dashed box. (b) The unitary U is efficiently implemented with the X and I (identity) gates, as described in the main text.

are small square matrices with elements $(\mathbf{M}_{0,0})_{nn'} = \langle u_{0n}\phi_n|\hat{H} - E|u_{0n'}\phi_{n'}\rangle$ and $(\mathbf{M}_{1,0})_{nn'} = \langle u_{0n}^*\phi_n|\hat{H} - E|u_{0n'}\phi_{n'}\rangle$ with $n, n' = 1, 2, ..., N_o$, where the basis functions are defined in eq 2. We follow the convention of ref 54 in assuming that the continuum basis functions $u_{0n}(R)$ and $u_{1n}(R)$ are not complex conjugated in the bra vectors. The $(N_l - 1)N \times N_o$ complex rectangular matrix $\mathbf{M}_0$ is composed of the elements $(\mathbf{M}_0)_{ln,n'} = \langle u_{ln}\phi_n|\hat{H} - E|u_{0n'}\phi_{n'}\rangle$ with n ranging from 1 to N and n' from 1 to N_o. Finally, $\mathbf{M}$ is a real symmetric matrix with dimensions $(N_l - 1)N \times (N_l - 1)N$ and elements $(\mathbf{M})_{ln,l'n'} = \langle u_{ln}\phi_n|\hat{H}-E|u_{l'n'}\phi_{n'}\rangle$.

Because eq 4 involves the inversion and multiplication of small $N_o \times N_o$ matrices $\mathbf{B}$ and $\mathbf{C}$, it may seem that the S-matrix can be computed efficiently on a classical computer. However, computing $\mathbf{B}$ and $\mathbf{C}$ using eq 5 requires the inversion of a large real symmetric matrix $\mathbf{M}$, which is the main computational bottleneck in computing the S-matrix in classical KVP.[51,54] Here, we overcome this bottleneck by using the VQLS, a recently proposed hybrid quantum-classical algorithm for solving linear systems of equations.[53]

The central strategy of the VQLS algorithm is to variationally prepare a quantum state $|x\rangle$ satisfying $\mathbf{A}|x\rangle \propto |b\rangle$ or, equivalently, $\mathbf{A}|x\rangle/\sqrt{\langle x|\mathbf{A}^\dagger\mathbf{A}|x\rangle} \approx |b\rangle$, where $\mathbf{A}$ is a real symmetric matrix and $|b\rangle$ is a normalized version of a vector $\vec{b}$. The Q-KVP method involves both the real and complex types of quantum linear systems in eqs 4 and (5): $\mathbf{B}^*|x\rangle = |b\rangle$ and $\mathbf{M}|x\rangle = |b\rangle$.

Inverting the matrix $\mathbf{M}$ amounts to solving a quantum linear systems problem, $\mathbf{M}\vec{x}_k = \vec{b}_k$, $k = 1, 2, ..., 2^n$, where n is the number of qubits, $\mathbf{M}$ is a real symmetric $2^n \times 2^n$ matrix, and $\vec{b}_k$ is a unit vector of $\mathbb{R}^{2^n}$ such that $\vec{b}_1 = (1, 0, 0, ..., 0)$, $\vec{b}_2 = (0, 1, 0, ..., 0)$, etc. Then, the vector $\vec{x}_k = \mathbf{M}^{-1}\vec{b}_k$ forms the k-th column of $\mathbf{M}^{-1}$. Using Dirac's notation, $\vec{x}_k \to |x_k\rangle$ and $\vec{b}_k \to |b_k\rangle$, we can recast the matrix $\mathbf{M}^{-1}$ as

$$\begin{pmatrix} \langle b_0|\mathbf{M}^{-1}|b_0\rangle & \langle b_0|\mathbf{M}^{-1}|b_1\rangle & \cdots & \langle b_0|\mathbf{M}^{-1}|b_{2^n}\rangle \\ \langle b_1|\mathbf{M}^{-1}|b_0\rangle & \langle b_1|\mathbf{M}^{-1}|b_1\rangle & \cdots & \langle b_1|\mathbf{M}^{-1}|b_{2^n}\rangle \\ \vdots & \vdots & \ddots & \vdots \\ \langle b_{2^n}|\mathbf{M}^{-1}|b_0\rangle & \langle b_{2^n}|\mathbf{M}^{-1}|b_1\rangle & \cdots & \langle b_{2^n}|\mathbf{M}^{-1}|b_{2^n}\rangle \end{pmatrix} = \begin{pmatrix} \langle b_0|x_0\rangle & \langle b_0|x_1\rangle & \cdots & \langle b_0|x_{2^n}\rangle \\ \langle b_1|x_0\rangle & \langle b_1|x_1\rangle & \cdots & \langle b_1|x_{2^n}\rangle \\ \vdots & \vdots & \ddots & \vdots \\ \langle b_{2^n}|x_0\rangle & \langle b_{2^n}|x_1\rangle & \cdots & \langle b_{2^n}|x_{2^n}\rangle \end{pmatrix}.$$

Thus, we need to solve a system of 2^n linear equations to get the complete representation of $\mathbf{M}^{-1}$.

In the framework of the VQLS algorithm,[53] we initially prepare four fundamental inputs: matrices $\mathbf{P}$, a gate $\mathbf{U}$, an ansatz $V(\theta)$, and a cost function C. First, we decompose $\mathbf{M}$ into a linear combination of unitary matrices $\mathbf{M}_l$.

The variational ansatz $V(\theta)$ is a unitary operator acting on n qubits, which depends on several parameters denoted collectively by θ. $V(\theta)|0\rangle$ represents an approximation to $|\vec{x}_k\rangle$, which solves the system of linear equations $\mathbf{M}\vec{x}_k = \vec{b}_k$, $k = 1, 2, ..., 2^n$. The most common types of VQE ansatzes used in computational quantum chemistry are hardware-efficient and chemically inspired ansatzes.[2,17,55−57] Here, as shown below, we employ a multiply layered hardware efficient ansatz composed of a sequence of single-qubit rotations (R_y gates) and two-qubit entangling CX gates as described in ref 58. Quantum gates realize single-qubit and two-qubit unitary transformations, which are elementary building blocks of any unitary transformation used in quantum algorithms.[9] Only the R_y gates contain parameters, whereas the CX gates do not. For an ansatz including one layer and three qubits, there are three variational parameters, θ_1, θ_2, and θ_3. Increasing the number of layers of ansatz will increase the numbers of parameters.

In general, we can choose $\mathbf{M}_l$ in the form of products of Pauli matrices $\mathbf{P}_l \in \{\mathbf{I}, \mathbf{X}, \mathbf{Y}, \mathbf{Z}\}^{\otimes n}$

$$\mathbf{M} = \sum_l c_l \mathbf{P}_l, \tag{6}$$

where the expansion coefficients are given by $c_l = (1/2^n)\,\mathrm{Tr}(\mathbf{M}\mathbf{P}_l)$.

Second, we create a parametrized quantum circuit using a multiply layered hardware efficient ansatz $V(\theta)$ such that our trial solution is of the form $|x(\theta)\rangle = V(\theta)|0\rangle$, where θ represents a set of variational parameters and $|0\rangle = |0\rangle^{\otimes n}$ is the initial state of n qubits (see Figure 1). A single layer in the dashed box in Figure 1 is a repeated sequence of quantum gates used in hardware-efficient ansatzes.[2,17] The number of layers gives the number of repeated gates sequences. While using more layers involves more parameters, which allows for more efficient optimization of the cost function $C(\theta)$, it also increases the computational cost (see Table 1). Each layer of the ansatz consists of single-qubit R_y gates and two-qubit CX gates. The number of layers is adjustable depending on the problem and also represents the depth of the ansatz.

Third, we prepare the quantum states $|b\rangle$ proportional to the vectors $\vec{b}$ on the right-hand side of $\mathbf{M}\vec{x}_k = \vec{b}_k$ (omitting the index k for simplicity) on a quantum circuit using an efficient gate sequence U shown in Figure 1b. The unitary transformation U is composed of only single-qubit identity (I) and

https://doi.org/10.1021/acs.jpclett.3c00985
J. Phys. Chem. Lett. 2023, 14, 6224−6233

Table 1. Fidelity $\mathcal{F}$ and Computing Time τ of Inverting the M Matrix for E = 3.8 for the SJ Problem with Two Open Channels[a]

k	$\mathcal{F}^1$	$\mathcal{F}^2$	$\mathcal{F}^3$	τ^1 (s)	τ^2 (s)	τ^3 (s)
1	0.1588	0.5834	0.9999	63.8	1355.4	2699.6
2	0.6446	0.9988	0.9999	84.5	1411.6	2657.3
3	0.8731	0.9884	0.9999	55.3	1865.9	3267.6
4	0.0925	0.9785	0.9999	80.7	1681.9	3872.4
5	0.0101	0.9999	0.9999	41.9	2155.7	2536.6
6	0.1232	0.9866	0.9999	105.4	2104.1	2227.5
7	0.9264	0.9967	0.9999	69.6	1787.7	3197.0
8	0.0058	0.9911	0.9999	55.7	1936.7	2838.1

[a]The superscript d of $\mathcal{F}^{(d)}$ and $\tau^{(d)}$ indicates the number of layers in the ansatz. The dimension of the M matrix is 8 × 8.

X gates. The structure of U depends on the number of qubits and the binary form of the number k. Specifically, we apply the I gate to each 0 digit in the binary representation of k and the X gate to each "1" digit. For instance, for 3 qubits, we have U = IXI for k = 2 (010), U = XXX for k = 7 (111), and so on (the binary representation of k is given in parentheses).

Finally, to obtain an optimal θ to ensure $\mathbf{M}|x(\theta)\rangle/\sqrt{\langle x(\theta)|\mathbf{M}^\dagger\mathbf{M}|x(\theta)} \approx |b\rangle$, we use the local version of the cost function in the VQLS algorithm[53]

$$C = 1 - \frac{|\langle b\Phi\rangle|^2}{\langle x(\theta)|\mathbf{M}^\dagger\mathbf{M}|x(\theta)\rangle}. \tag{7}$$

where $|\Phi\rangle = \mathbf{M}\,|x(\theta)\rangle$. Combining eqs 6 and 7, the cost function becomes

$$C = 1 - \frac{\sum_{ll'} c_l c_{l'}^* \langle 0|U^\dagger \mathbf{P}_{l'} V(\theta)|0\rangle\langle 0|V(\theta)^\dagger \mathbf{P}_l^\dagger U|0\rangle}{\sum_{ll'} c_l c_{l'}^* \langle 0|V(\theta)^\dagger \mathbf{P}_{l'}^\dagger \mathbf{P}_l V(\theta)|0\rangle} \tag{8}$$

Here, $U|0\rangle$ and $|0\rangle\langle 0|$ are replaced by $|b\rangle$ and $\mathbf{O} = \frac{1}{2} + \frac{1}{2n}\sum_{j=0}^{n-1}\mathbf{Z}_j$, respectively, in order to make the estimation of expectation values easier, and the Pauli $\mathbf{Z}$ operator is locally implemented on the j-th qubit (j = 0, 1, ..., n − 1).

By minimizing the cost function, we obtain the optimal variational parameters θ and the optimal solution $|x\rangle$= $|x(\theta)\rangle$= $V(\theta)\,|0\rangle$, which satisfies $\mathbf{M}|x(\theta)\rangle/\sqrt{\langle x(\theta)|\mathbf{M}^\dagger\mathbf{M}|x(\theta)\rangle} \approx |b\rangle$. As the ansatz $V(\theta)$ is unitary, $|x(\theta)\rangle$ has a unit norm. The vector $\vec{x} = \mathcal{N}_q|x(\theta)\rangle$ has the quantum norm $\mathcal{N}_q = |||b\rangle||/||\mathbf{M}|x(\theta)\rangle||$, which is expected to be close to the exact classical norm $\mathcal{N}_c = ||\vec{x}||$ (the difference between $\mathcal{N}_q$ and $\mathcal{N}_c$ is quantified by the fidelity, see below). Finally, we assemble matrix $\mathbf{M}^{-1}$ from the solution vectors. The sign of $\vec{x}$ is determined by requiring $\mathbf{M}\mathbf{M}_q^{-1} = \mathbf{I}$. The above-mentioned steps of the Q-KVP method are illustrated in Figure 2.

We begin by applying the Q-KVP algorithm to a model single-channel quantum scattering problem described by the Hamiltonian

$$\hat{H} = -\frac{1}{2\mu}\frac{d^2}{dR^2} + V(R), \tag{9}$$

where $V(R) = -e^{-R}$.[54] To this end, we define a single-channel ansatz

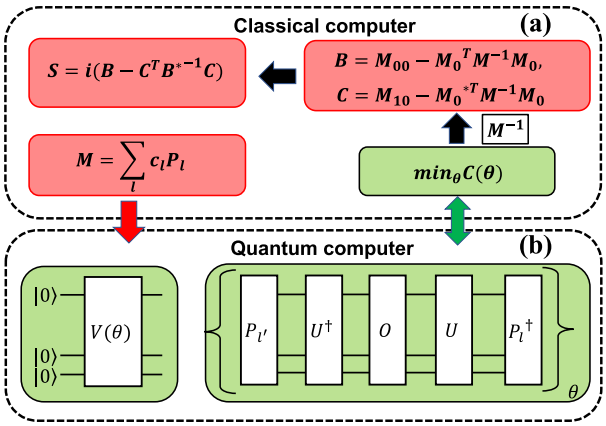

Figure 2. Schematic diagram of the hybrid Q-KVP algorithm.

$$\psi_t(R) = -u_0(R) + c_1 u_1(R) + \sum_{l=2}^{N_l} c_l u_l(R), \tag{10}$$

where $k = \sqrt{2\mu E}$ is the wavenumber, E is the total energy, $v = k/\mu$ is the asymptotic velocity, $u_0 = f(R)e^{ikR}v^{-1/2}$, $f(R)$ is the cutoff function defined above, and $u_1(R) = u_0(R)^*$. We take the bound-state basis functions to be $u_l(R) = F_l R^{l-1} e^{-\gamma R}$ (l = 2, 3, ..., N_l), and define the matrix elements

$$M_{00} = \langle u_0|\hat{H} - E|u_0\rangle,\ M_{10} = \langle u_1|\hat{H} - E|u_0\rangle;$$

$$(\mathbf{M}_0)_l = \langle u_l|\hat{H} - E|u_0\rangle,\ (\mathbf{M})_{ll'} = \langle u_l|\hat{H} - E|u_{l'}\rangle,$$

where M_{00} and M_{10} are complex scalars, $\mathbf{M}_0$ is a complex vector, and $\mathbf{M}$ is a real symmetric square matrix (see above). Substituting these expressions into eq 5, we obtain the S matrix element, which, for single-channel scattering, is a complex number of unit magnitude ($|S|^2$ = 1). The bound-state basis functions $u_l(R)$ are parametrized by γ = 1.5, and we take μ = 1 au.

To compute the S-matrix using the Q-KVP algorithm, we start by inverting the $\mathbf{M}$-matrix in the framework of the VQLS algorithm on the Qiskit platform. The quality of the unit vectors $|x_q\rangle$= $|x(\theta)\rangle$ obtained using VQLS is measured by the fidelity

$$\mathcal{F}_{qc} = |\langle x_q|x_c\rangle|^2, \tag{11}$$

which is a squared overlap between $|x_q\rangle$ and the exact result, $|x_c\rangle = \vec{x}/\mathcal{N}_c$, obtained by a classical inversion method. We obtain fidelities very close to 1 using an ansatz with two layers as discussed in more detail in the Supporting Information.[9]

Figure 3 shows the collision energy dependence of the real and imaginary parts of the S-matrix calculated using our Q-KVP approach. The quantum results are in excellent agreement with the benchmark values obtained by direct numerical integration of the Schrödinger equation on a classical computer using the numerically exact coupled channel (CC) method[59] over the whole range of collision energies. As a point of reference, at k = 0.55, our Q-KVP calculations give S = −0.65714 + i0.75633 for N_l = 2, which compares favorably with the exact CC result (S = − 0.65769 + i0.75328). Increasing the number of basis functions to 4 changes the imaginary part of the S-matrix element by only 0.4% (and its real part by much less), indicating good convergence of the Q-KVP results.

https://doi.org/10.1021/acs.jpclett.3c00985
J. Phys. Chem. Lett. 2023, 14, 6224−6233

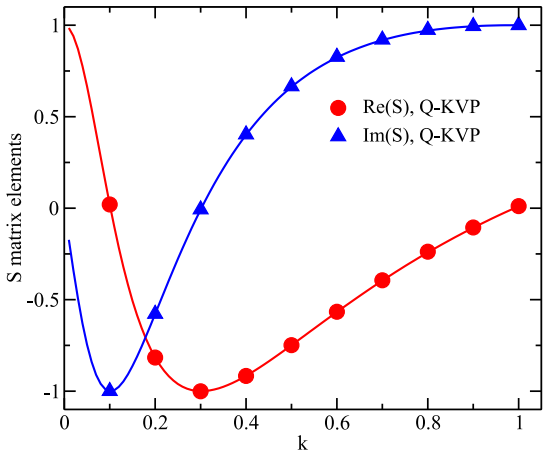

Figure 3. Real and imaginary parts of the S-matrix plotted as a function of the relative wavevector k. Symbols: Q-KVP results calculated with $N_l = 2$. Solid lines: benchmark results computed using the CC method on a classical computer. The error bars on the quantum results are much smaller than the size of the symbols.

To explore the applicability of the Q-KVP algorithm to more realistic (and more complex) multichannel quantum scattering problems, we apply it to solve a two-dimensional Secrest–Johnson (SJ) model,[60,61] which describes collinear collisions of a diatomic molecule with a structureless atom. The molecule is approximated by a harmonic oscillator, and a model two-dimensional (2D) potential function is used to describe the atom–molecule interaction (see below). Because of these features, the SJ model is significantly more complex than the one-channel problem considered in the previous section, and it continues to serve as a benchmark for testing new methods for solving CC equations of quantum scattering theory.[62]

The Hamiltonian of the SJ model is, in reduced coordinates[60,61]

$$\hat{H} = -\frac{1}{2\mu}\frac{\partial^2}{\partial R^2} + V(R, r) - \frac{1}{2m}\frac{\partial^2}{\partial r^2} + \frac{1}{2}r^2, \tag{12}$$

where R is the scaled distance between the atom and the molecule's center of mass, r is the scaled internuclear distance in the molecule, μ is proportional to the reduced mass of the atom–molecule system, and we use the values $m = 1$ and $\mu = 0.6667$, which correspond to He + H_2 collisions.[60,61] The Hamiltonian includes the kinetic energy of the atom relative to the molecule (the first term), the atom–molecule interaction potential (the second term), and the vibrational energy of the diatomic molecule (the third and fourth terms).

The atom–molecule interaction potential $V(R, r)$ in the SJ model has the form

$$V(R, r) = Ae^{-\alpha R + \beta r}, \tag{13}$$

where A is a constant, which defines the classical turning point for the collision, and the parameters α and β characterize the exponential decay of the potential with R and its dependence on the diatomic stretching coordinate r. To parametrize the interaction potential, we choose the values $A = 10$, $\beta = 2$, and $\alpha = 0.3$. The scattering wave function $|\psi_t\rangle$ satisfies the time-independent Schrödinger equation $\hat{H}|\psi_t\rangle = \frac{1}{2}E|\psi_t\rangle$, where the total energy E is expressed in units of the zero-point vibrational energy of the diatomic molecule.[60]

We choose the Q-KVP ansatz for $|\psi_t\rangle$ in the form of eq 2 with the transitional wave functions given by eq 3 with $\gamma = 0.5$. The internal wave functions $\phi_n(r)$ are the vibrational wave functions of the harmonic oscillator $\phi_v(r)$, where v is the vibrational quantum number. Because $V(R, r) \to 0$ as $R \to \infty$, the threshold energies of the vibrational channels are given by the energy levels of the one-dimensional harmonic oscillator, $\epsilon_v = v + 1/2$. As noted above, the dimension of the S matrix is equal to the number of open channels, N_o. To avoid the overcompleteness problem caused by nonorthogonality of the basis functions $|u_{ln}\phi_n\rangle$, we transform the matrix $\mathbf{M}$ to an orthonormal basis as described in the SI.[9] The transformed matrices have the dimensions $N_q \times N_q$ for M and $N_q \times N_o$ for $\mathbf{M}_0$, where N_q is the number of orthogonalized basis functions.

Table 1 lists the fidelities for inverting the $\mathbf{M}$-matrix using VQLS in the basis of 8 orthogonalized functions. The fidelity $\mathcal{F}^{(d)}$ is computed for ansatzes in Figure 1a with varying numbers of layers d (for depth). We observe that a single-layer ansatz cannot provide consistently good fidelity for all columns k of $\mathbf{M}^{-1}$. The values of $\mathcal{F}^{(1)}$ vary from 0.0925 to 0.9264. Increasing the depth of the ansatz leads to a dramatic improvement in inversion fidelity; values of $\mathcal{F}^{(3)} = 0.9999$ are obtained using only three layers. A downside of using the $d \geq 3$ ansatzes is that their computational time increases rapidly. As shown in Table 1, the computational cost of $\tau^{(3)}$ is nearly 50 times greater than that of $\tau^{(1)}$. Thus, inverting a general (i.e., nonsparse) $2^n \times 2^n$ $\mathbf{M}$ matrix using the VQLS algorithm on the Qiskit platform is very costly for $n \geq 4$. This is partly because for a general, nonsparse matrix $\mathbf{M}$ the number of terms in its expansion in products of Pauli matrices (6) grows exponentially with matrix size. In order to avoid the explosive scaling, one should ensure that the number of Pauli terms grows only polynomically with the system size. This important question is addressed below.

Figure 4 compares the quantum and classical transition probabilities for collision-induced vibrational relaxation ($|S_{10}|^2$). We consider the case of a diatomic molecule initially in the $v = 1$ vibrational state colliding with a spherically symmetric atom, where the molecule can either scatter

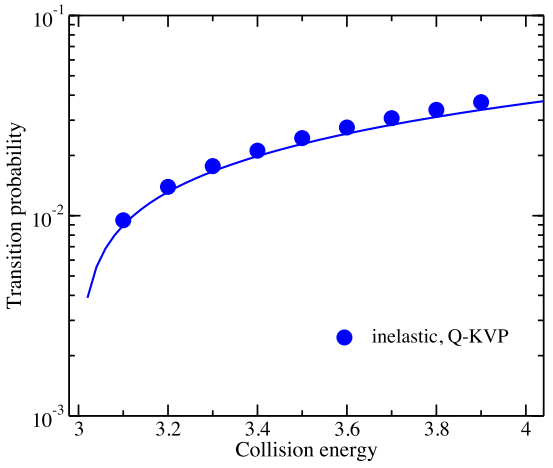

Figure 4. Transition probability for the inelastic collisional relaxation plotted as a function of collision energy for the case of two open channels ($v = 0, 1$). The size of the $\mathbf{M}$ matrix is 8×8. Solid symbols: Q–KVP results. Solid lines: reference results computed using exact CC.

https://doi.org/10.1021/acs.jpclett.3c00985
J. Phys. Chem. Lett. 2023, 14, 6224–6233

elastically or undergo vibrational relaxation to the $v = 0$ ground state. The Q-KVP calculations use the **M** matrix in a basis of 8 orthogonalized basis functions, each of which is expanded in 12 primitive basis functions $|u_{l_n}\phi_n\rangle$ (see the Supporting Information[9]). The quantum probabilities are in very good agreement with exact CC calculations at all collision energies, validating our Q-KVP approach. In particular, the monotonic increase in the transition probability with collision energy is well reproduced by quantum calculations.

Having compared the inelastic transition probabilities, we now turn to the underlying complex transition amplitudes. Figure 5 shows the real and imaginary parts of the elastic and

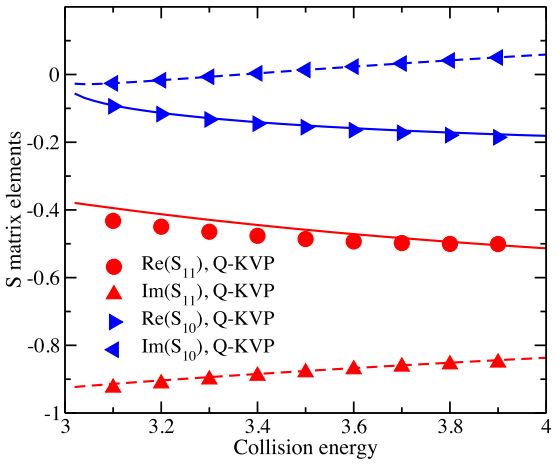

Figure 5. Real and imaginary parts of the S-matrix plotted as a function of collision energy for the SJ model. Two channels are open ($v = 0, 1$), and the size of the **M** matrix is 8 × 8. Symbols: Q−KVP results. Solid lines: reference results computed using exact CC.

inelastic amplitudes (S_{11} and S_{10}) obtained from our Q-KVP calculations. As in the case of transition probabilities (Figure 4), we observe excellent agreement between the Q-KVP and exact CC inelastic *S*-matrix elements at all collision energies. However, the elastic S-matrix element ($\mathrm{Re}(S_{11})$) deviates slightly from the exact CC result at lower energies. This is likely due to the limited size of our basis set, which contains 8 orthogonalized basis functions.

To demonstrate the scalability of the Q-KVP algorithm, (i.e., its ability to solve large-scale molecular scattering problems with exponential speedup over classical algorithms) we need to find a representation of the scattering Hamiltonian (or, equivalently, of **M**) that is *k*-local, i.e., with each $\mathbf{P}_l$ term in eq 6 acting in a nontrivial way on no more than *k* qubits.[1] If this condition is met, the number of Pauli terms will grow polynomially with the size of the system, enabling efficient digital quantum simulation.[1,2,17] To this end, consider the Cartesian reaction path Hamiltonian that describes a wide range of molecular quantum scattering processes, including inelastic collisions, quantum reactive scattering, and isomerization[63−66]

$$\hat{H} = \sum_i \frac{P_i^2}{2M_i} + \sum_i \left[\frac{p_i^2}{2m_i} + \frac{1}{2}m_i\omega_i^2(y_i - y_{i_0})^2\right] + V(\mathbf{R}, \mathbf{y}), \tag{14}$$

where the Cartesian coordinates $\mathbf{R} = (R_1, R_2, ...)$ describe the large-amplitude motion of molecular fragments responsible for the chemical reaction or inelastic scattering, whereas the coordinates **y** describe the majority of molecular degrees of freedom that only exhibit small (nearly harmonic) displacements described by the harmonic Hamiltonians $\hat{H}_i = \frac{p_i^2}{2m_i} + \frac{1}{2}m_i\omega_i^2(y_i - y_{i_0})^2$. Accordingly, the adiabatic interaction potential energy surface can be expanded in these displacements[63,67] (assuming the validity of the Born−Oppenheimer approximation)

$$V(\mathbf{R}, \mathbf{y}) = V(\mathbf{R}, \mathbf{y}_0) + \sum_{i=1}^{N_M} K_i^{(1)}(\mathbf{R})(y_i - y_{i_0}) + \sum_{i\neq j}^{N_M} K_{ij}^{(2)}(\mathbf{R})(y_i - y_{i_0})(y_j - y_{j_0}) + ..., \tag{15}$$

where $V(\mathbf{R}, \mathbf{y}_0)$ is the value of the interaction potential at the reference geometry with all vibrational degrees of freedom frozen at their equilibrium positions y_{i_0}, N_M is the number of vibrational modes, and $K_{i_1 i_2 \ldots i_n}^{(n)}$ are the expansion coefficients given by the *n*-th order derivatives of the interaction potential with respect to $y_{i_1}, y_{i_2}, ..., y_{i_n}$, i.e. $K_{ij}^{(2)} = \frac{1}{2}\frac{\partial^2 V(\mathbf{R},\mathbf{y})}{\partial y_i \partial y_j}|_{\mathbf{y}=\mathbf{y}_0}$. Because the Cartesian reaction path Hamiltonian (14) is an extension of the vibrational Hamiltonian describing small-amplitude vibrations of polyatomic molecules, solving it beyond the harmonic approximation is a hard problem for classical computers.[17]

To recast the Hamiltonian (14) into a *k*-local form, we choose an orthonormal direct-product basis set $|u_l\rangle|\phi_{v_1}^{(1)}\phi_{v_2}^{(2)}...\phi_{v_M}^{(N_M)}\rangle$ composed of N_R scattering basis functions $\langle R|u_l\rangle = u_l(R)$ and $N_v^{N_M}$ vibrational basis functions $|\phi_{v_1}^{(1)}\rangle$, $|\phi_{v_2}^{(2)}\rangle$, ..., $|\phi_{v_M}^{(N_M)}\rangle$ (with N_v functions per each vibrational mode). For simplicity, we consider the case of a single scattering variable, *R*, which describes inelastic scattering or chemical reactions dominated by a single reaction coordinate. The operator $\hat{H} - E = \hat{H}(E)$ then becomes

$$\hat{H}(E) = \sum_{l,l'}\sum_{\substack{v_1,v_2,\ldots \\ v_1',v_2',\ldots}} (|u_l\rangle\langle u_{l'}|)|\phi_{v_1}^{(1)}\phi_{v_2}^{(2)}...\rangle\langle\phi_{v_1'}^{(1)}\phi_{v_2'}^{(2)}...| \langle\phi_{v_1}^{(1)}\phi_{v_2}^{(2)}...|\hat{H}(E)|\phi_{v_1'}^{(1)}\phi_{v_2'}^{(2)}...\rangle|u_{l'}\rangle \tag{16}$$

with the matrix elements of the Hamiltonian (14) given by

$$\begin{aligned}
&\langle u_l|\langle\phi_{v_1}^{(1)}\phi_{v_2}^{(2)}...|\hat{H}(E)|\phi_{v_1'}^{(1)}\phi_{v_2'}^{(2)}...\rangle|u_{l'}\rangle \\
&= \delta_{v_1v_1'}\delta_{v_2v_2'}...\left[\langle u_l|\frac{P^2}{2M} - E + V(R, \mathbf{y}_0)|u_{l'}\rangle\right] \\
&\quad + \delta_{ll'}\langle\phi_{v_1}^{(1)}\phi_{v_2}^{(2)}...|\sum_i \hat{H}_i|\phi_{v_1'}^{(1)}\phi_{v_2'}^{(2)}...\rangle \\
&\quad + \sum_{i=1}^{N_M}\langle u_l|K_i^{(1)}(R)|u_{l'}\rangle\delta_{v_1v_2...;v_1'v_2'...}^{(i)}\langle\phi_{v_i}^{(i)}|(y_i - y_{i_0})|\phi_{v_i'}^{(i)}\rangle \\
&\quad + \sum_{i,j=1}^{N_M}\langle u_l|K_{ij}^{(2)}(R)|u_{l'}\rangle\delta_{v_1v_2...;v_1'v_2'...}^{(ij)}\langle\phi_{v_i}^{(i)}|(y_i - y_{i_0})|\phi_{v_i'}^{(i)}\rangle \\
&\quad \langle\phi_{v_j}^{(j)}|(y_j - y_{j_0})|\phi_{v_j'}^{(j)}\rangle + ...
\end{aligned} \tag{17}$$

https://doi.org/10.1021/acs.jpclett.3c00985
J. Phys. Chem. Lett. 2023, 14, 6224−6233

where we have included all the terms up to the second order [higher-order anharmonic terms have a similar structure involving sums of products of the matrix elements of $K_{i_1 i_2,\ldots,\ i_n}^{(n)}(R)$]. In eq 17, $\delta_{v_1,v_2,\ldots;\ v_1' v_2' \ldots}^{(i)}$ denotes the product of $N_M - 1$ Kronecker delta symbols $\delta_{v_1 v_1'}\delta_{v_2\ v_2'}\ldots$, which does not include $\delta_{v_i v_i'}$ and $\delta_{v_1,v_2\ldots;\ v_1' v_2' \ldots}^{(ij)}$ stands for the product of $N_M - 2$ Kronecker delta symbols, which does not include $\delta_{v_i v_i'}$ and $\delta_{v_j v_j'}$. Combining eqs 16 and 17, we obtain the Pauli decomposition of the scattering Hamiltonian

$$
\begin{aligned}
\hat{H} - E = {} & \mathbf{H}^{(R)} \otimes \mathbf{1}^{(v_1)} \otimes \ldots + \mathbf{1}^{(R)} \otimes \\
& \sum_{i=1}^{N_M} [\ldots \otimes \mathbf{1}^{v_{(i-1)}} \otimes \mathbf{E}^{(v_i)} \otimes \mathbf{1}^{(v_{i+1})} \otimes \ldots] \\
& + \sum_{i=1}^{N_M} \left(\sum_{i_1,i_2,\ldots\,\alpha_1,\alpha_2,\ldots} k_{i,\alpha_1\alpha_2\ldots}^{(1) i_1 i_2 \ldots} \sigma_{\alpha_1}^{i_1} \sigma_{\alpha_2}^{i_2} \ldots \right) \otimes \mathbf{1}^{(v_1)} \otimes \\
& \ldots \otimes \mathbf{y}_i^{(v_i)} \otimes \\
& \ldots + \sum_{i,j=1 i \neq j}^{N_M} \left(\sum_{i_1,i_2,\ldots\,\alpha_1,\alpha_2,\ldots} k_{ij,\alpha_1\alpha_2\ldots}^{(2) i_1 i_2 \ldots} \sigma_{\alpha_1}^{i_1} \sigma_{\alpha_2}^{i_2} \ldots \right) \otimes \mathbf{1}^{(v_1)} \\
& \otimes \ldots \otimes \mathbf{y}_i^{(v_i)} \otimes \ldots \otimes \mathbf{y}_j^{(v_j)} \otimes \\
& \ldots + \sum_{i=1}^{N_M} \left(\sum_{i_1,i_2,\ldots\,\alpha_1,\alpha_2,\ldots} k_{ii,\alpha_1\alpha_2\ldots}^{(2) i_1 i_2 \ldots} \sigma_{\alpha_1}^{i_1} \sigma_{\alpha_2}^{i_2} \ldots \right) \otimes \mathbf{1}^{(v_1)} \otimes \\
& \ldots \otimes (\mathbf{y}_i^2)^{(v_i)} \otimes \ldots + \text{anharmonic terms}, \qquad (18)
\end{aligned}
$$

where $\mathbf{1}_R$ and $\mathbf{1}^{(v_i)}$ are unit operators in the scattering space spanned by $N^{(R)}$ basis functions $|u_l\rangle$, and in the Hilbert space of the v_i-th vibrational mode spanned by N_v vibrational basis functions $|\phi_{v_i}^{(i)}\rangle$, $\mathbf{H}^{(R)} = \sum_{\substack{i_1,i_2,\ldots \\ \alpha_1,\alpha_2,\ldots}} u_{\alpha_1\alpha_2\ldots}^{i_1 i_2 \ldots} \sigma_{\alpha_1}^{i_1} \sigma_{\alpha_2}^{i_2} \ldots$ is the matrix representation of the first term of the Hamiltonian (17) expanded in Pauli matrices acting on $n_S = \log(N_R)$ "scattering" qubits α_1, α_2, ... Further, $\mathbf{E}^{(v_i)} = \mathrm{diag}(E_0^{(i)}, E_1^{(i)}, \ldots)$ are the diagonal matrices of vibrational energies of the i-th mode, and $k_{i,\alpha_1\alpha_2\ldots}^{(i)\ i_1 i_2 \ldots}$ and $k_{ij,\alpha_1\alpha_2\ldots}^{(2)\ i_1 i_2 \ldots}$ are the expansion coefficients in the Pauli decomposition (6) of the matrices $(\mathbf{K}^{(i)})_{ll'} = \langle u_l | K_i^{(1)}(R) | u_{l'} \rangle$ and $(\mathbf{K}^{(ij)})_{ll'} = \langle u_l | K_{ij}^{(2)}(R) | u_{l'} \rangle$. The number of terms in these expansions generally scales as $O(N_T^R) = O(2^{N_R})$. This does not pose a fundamental problem, however, because the number of reaction coordinates typically ranges from one to three for most chemical reactions of interest[63] regardless of system size. Importantly, therefore, the presence of a large number of terms in the Pauli expansions of $\mathbf{H}^{(R)}$, $\mathbf{K}^{(i)}$, and $\mathbf{K}^{(ij)}$ does not affect the overall scaling with the system size of the number of terms in eq 18, which is determined instead by the much more numerous vibrational modes (see below). Finally, the $N_v \times N_v$ matrices $(\mathbf{y}_i^n)^{(v_i)}$ in eq 18 are given by $\{(\mathbf{y}_i^n)^{(v_i)}\}_{v_i v_i'} = \langle \phi_{v_i}^{(i)} | (y_i - y_{i_0})^n | \phi_{v_i'}^{(i)} \rangle$.

To encode vibrational modes into the "vibrational qubits" labeled (v_1), (v_2), ..., we will use a compact mapping, which requires $n_v = \log N_v$ qubits per mode,[17] where the Pauli decompositions of matrices $\mathbf{E}^{(i)}$ and $(\mathbf{y}_i^n)^{(v_i)}$ contain only $O(N_v^2)$ and $O(N_v^{2n})$ terms, respectively. This implies that the total number of terms in the Pauli expansion of the scattering Hamiltonian (18) scales polynomially as $O(N_T^R) \times N_M^2 \times O(N_v^{2n})$ with the number of vibrational modes N_M and the number of vibrational basis functions per mode N_v. The k-locality of the Cartesian reaction path Hamiltonian (14) suggests that it could be efficiently simulated on a quantum computer. If m-th order anharmonic terms are included in the expansion of the interaction potential (15), then the scaling becomes steeper $[O(N_T^R) \times N_M^m \times O(N_v^{2m})]$ but remains polynomial for any finite m. The inclusion of anharmonic effects is important for large polyatomic molecules; therefore, it will be essential to keep m as small as possible to reduce the computational cost.

Table 2 lists the estimated number of qubits and Pauli terms required for the digital quantum simulation of quantum collision dynamics of medium-to-large molecules ethylene (C_2H_4), benzene (C_6H_6), and naphthalene ($C_{10}H_8$). Collisions involving such hydrocarbon molecules play an important role in combustion and possibly in the interstellar medium,[27] and pose an intriguing "sticking" problem[68−70] concerning the role of molecular vibrations in the formation of long-lived collision complexes. The problem is described by a single scattering coordinate, R, the distance between the molecules' centers of mass. The number of small-amplitude vibrational modes of the collision complex is thus $N_M = (3N_a - 3) - 1 - N_A$, where N_a is the total number of nuclei and $N_A = 8$ is the number of angular variables, including six Euler angles that specify the position of each nonlinear molecule with respect to the intermolecular axis $\mathbf{R}$ and the two angles that determine the orientation of $\mathbf{R}$ in the laboratory frame.

Table 2. Estimated Number of Qubits $n_q = n_S + N_M\, n_v$ and Pauli Terms $N_P = N_T^R N_M^2 N_v^4$ for Simulating Collisions of Ethylene (C_2H_4), Benzene (C_6H_6), and Naphthalene ($C_{10}H_8$) Molecules[a]

collision	n_q	$N_P \times 10^3$
$C_2H_4 + C_2H_4$	26	147.5
$C_6H_6 + C_6H_6$	62	921.6
$C_{10}H_8 + C_{10}H_8$	98	2,560

[a]The basis set includes 4 scattering states ($N_R = 2$, $N_T^R = 16$) encoded in 2 scattering qubits ($n_S = 2$), and 2 vibrational basis functions ($N_v = 2$) encoded into 1 qubit per vibrational mode ($n_v = 1$). eq 18 is truncated at the harmonic level ($m = 2$). Rotational degrees of freedom are neglected for simplicity since they are greatly outnumbered by vibrations already for medium-size molecules,[63] and thus do not affect the scaling of scattering computations with system size.

An important future challenge to achieving quantum advantage for large scattering problems will be the storage of $2^n \times 2^n$ $\mathbf{M}^{-1}$ matrices, which are too large to be handled on a classical computer. To begin to address this challenge, we note that storing the entire matrix $\mathbf{M}^{-1}$ is not necessary because what is needed for the calculation of the S-matrix is the product $\mathbf{B} = \mathbf{M}_0^T \mathbf{M}^{-1} \mathbf{M}_0$, where $\mathbf{M}_0$ is a rectangular matrix of dimension $2^n \times N_o$, and N_o is a small number of open channels. The columns of the rectangular matrix $\mathbf{X} = \mathbf{M}^{-1}\mathbf{M}_0$ are solutions to the system of linear equations $\mathbf{MX} = \mathbf{M}_0$. Thus, if one can prepare the rectangular matrix $\mathbf{M}_0$ (composed of N_o vectors of dimension 2^n) on a quantum computer, then the VQLS algorithm can be used to obtain the circuit representation of $\mathbf{X}$ and then of $\mathbf{B}$ and $\mathbf{S}$ without explicitly inverting the $2^n \times 2^n$ matrix $\mathbf{M}$. To prepare the columns of $\mathbf{M}_0$ on a quantum computer, one can use the recently developed

https://doi.org/10.1021/acs.jpclett.3c00985
J. Phys. Chem. Lett. 2023, 14, 6224−6233

algorithms for quantum state initialization.[71−73] While this is a nontrivial task beyond the scope of this work, it may be possible to leverage the properties of $\mathbf{M}_0$ to increase the efficiency of the initialization procedure.

Another way to avoid reconstructing the full $\mathbf{M}^{-1}$ matrix is to bypass the matrix inversion procedure altogether. Instead, we can begin with the S-matrix functional (1) and directly vary the parameters of the trial functions $\tilde{\psi}_{n_i}(c_{ln,n_i})$ and $\tilde{\psi}_{n_f}(c_{ln,n_f})$ until an extremum of $S_{n_f\, n_i}$ is found. This *direct extremization* procedure is similar in spirit to the original VQE approach[13] with one significant difference: To find the *S*-matrix, we need to extremize the complex functional (1), rather than to minimize a real functional as done in the VQE. This can be achieved by extremizing the real and imaginary parts of $S_{n_f\, n_i}(c_{lm,n})$ in eq 1 while maintaining its unitarity, $\sum_k S^{\dagger}_{n\, k} S_{kn'} = \sum_k S_{nk} S^{\dagger}_{kn'} = \delta_{nn'}$. One can implement the previously developed trial functions to calculate the expectation value in eq 1 such as the unitary vibrational coupled cluster (UVCC) ansatz proposed for calculating the eigenstates of the vibrational Hamiltonian using the VQE.[17]

In conclusion, we proposed a hybrid classical-quantum algorithm for the solution of multichannel quantum scattering problems, which are ubiquitous not only in physical chemistry but also in atomic and molecular physics. The Q-KVP algorithm combines the *S*-matrix version of the Kohn variational principle (KVP)[54] and the recently developed VQLS algorithm[53] to address the major computational bottleneck of the classical KVP algorithm, the inversion of a large real symmetric matrix M. The use of VQLS to accomplish the inversion represents the key connection between the scattering theory and quantum computing parts of this work. The inverted matrix $\mathbf{M}^{-1}$ is then used to obtain the scattering *S*-matrix using eqs 4 and 5.

In our initial implementation of the Q-KVP methodology on a classical emulator of quantum hardware using Qiskit in Python, we construct a $2^n \times 2^n$ matrix $\mathbf{M}$ using an orthogonalized finite basis set and invert it using hardware-efficient multilayered ansatzes. This procedure gives accurate results for both single- and multichannel quantum scattering. We applied Q-KVP methodology to study vibrational energy transfer in collinear atom−diatom collisions using the archetypal SJ model. The vibrational transition probabilities computed using Q-KVP are in excellent agreement with the exact CC calculations, demonstrating the validity and accuracy of the Q-KVP methodology. A current limitation of our approach is the large computational cost of inverting $\mathbf{M}$-matrices of dimensions ≥ 16 on the Qiskit platform, which precludes scattering computations at collision energies higher than those shown in Figure 4. We note that few-qubit implementations of other quantum inversion algorithms have also been limited to 8×8 matrices.[74] This is partly due to the exponentially increasing number of terms in the Pauli matrix expansion of $\mathbf{M}$. To address this limitation, we propose a scenario of how the Q-KVP algorithm could be scaled up to larger inelastic collisions or reactive scattering problems involving larger polyatomic molecules. This is achieved by explicitly expanding the few anharmonic (scattering) degrees of freedom in Pauli matrices and using the compact mapping for the remaining harmonic degrees of freedom as done in previous work on the digital quantum simulation of vibrational energy levels.[17]

■ ASSOCIATED CONTENT

Supporting Information

The Supporting Information is available free of charge at https://pubs.acs.org/doi/10.1021/acs.jpclett.3c00985.

More information on quantum computing and quantum gates, details of convergence tests, and additional information on the implementation of the VQLS and for the basis set orthogonalization procedure(PDF)

■ AUTHOR INFORMATION

Corresponding Author

Timur V. Tscherbul − *Department of Physics, University of Nevada, Reno, Nevada 89557, United States;* orcid.org/0000-0001-5689-040X; Email: ttscherbul@unr.edu

Authors

Xiaodong Xing − *Department of Physics, University of Nevada, Reno, Nevada 89557, United States;* orcid.org/0000-0001-6933-7048

Alejandro Gomez Cadavid − *Chemical Physics Theory Group, Department of Chemistry, University of Toronto, Toronto, Ontario M5S 3H6, Canada; Department of Physical and Environmental Sciences, University of Toronto Scarborough, Toronto, Ontario M1C 1A4, Canada; Kipu Quantum, Berlin 10405, Germany*

Artur F. Izmaylov − *Chemical Physics Theory Group, Department of Chemistry, University of Toronto, Toronto, Ontario M5S 3H6, Canada; Department of Physical and Environmental Sciences, University of Toronto Scarborough, Toronto, Ontario M1C 1A4, Canada;* orcid.org/0000-0001-8035-6020

Complete contact information is available at: https://pubs.acs.org/10.1021/acs.jpclett.3c00985

Notes

The authors declare no competing financial interest.

■ ACKNOWLEDGMENTS

We thank Robert Parrish for illuminating discussions. This work was supported by the NSF through the CAREER program (PHY-2045681). A.F.I. is grateful to the Mitacs Globalink program and the Natural Science and Engineering Council (NSERC) of Canada for financial support.

■ REFERENCES

(1) Cao, Y.; Romero, J.; Olson, J. P.; Degroote, M.; Johnson, P. D.; Kieferová, M.; Kivlichan, I. D.; Menke, T.; Peropadre, B.; Sawaya, N. P. D.; et al. Quantum Chemistry in the Age of Quantum Computing. *Chem. Rev.* **2019**, *119*, 10856−10915.

(2) McArdle, S.; Endo, S.; Aspuru-Guzik, A.; Benjamin, S. C.; Yuan, X. Quantum computational chemistry. *Rev. Mod. Phys.* **2020**, *92*, No. 015003.

(3) Argüello-Luengo, J.; González-Tudela, A.; Shi, T.; Zoller, P.; Cirac, J. I. Analogue quantum chemistry simulation. *Nature* **2019**, *574*, 215−218.

(4) Otten, M.; Hermes, M. R.; Pandharkar, R.; Alexeev, Y.; Gray, S. K.; Gagliardi, L. Localized Quantum Chemistry on Quantum Computers. *J. Chem. Theory Comput.* **2022**, *18*, 7205−7217.

(5) Fan, Y.; Liu, J.; Li, Z.; Yang, J. Equation-of-Motion Theory to Calculate Accurate Band Structures with a Quantum Computer. *J. Phys. Chem. Lett.* **2021**, *12*, 8833−8840.

(6) Colless, J. I.; Ramasesh, V. V.; Dahlen, D.; Blok, M. S.; Kimchi-Schwartz, M. E.; McClean, J. R.; Carter, J.; de Jong, W. A.; Siddiqi, I.

Computation of Molecular Spectra on a Quantum Processor with an Error-Resilient Algorithm. *Phys. Rev. X* **2018**, *8*, No. 011021.
(7) Parrish, R. M.; Hohenstein, E. G.; McMahon, P. L.; Martínez, T. J. Quantum Computation of Electronic Transitions Using a Variational Quantum Eigensolver. *Phys. Rev. Lett.* **2019**, *122*, 230401.
(8) Leontica, S.; Tennie, F.; Farrow, T. Simulating molecules on a cloud-based 5-qubit IBM-Q universal quantum computer. *Commun. Phys.* **2021**, *4*, 112.
(9) See the Supporting Information associated with this article for details of convergence tests, additional information on the implementation of the VQLS, and for the basis set orthogonalization procedure.
(10) Kitaev, A. Yu., Quantum measurements and the Abelian Stabilizer Problem. *arXiv:quant-ph/9511026*
(11) Nielsen, M. A.; Chuang, I. L. *Quantum Computation and Quantum Information: 10th Anniversary Edition*; Cambridge University Press: 2010.
(12) Pezzè, L.; Smerzi, A. Quantum Phase Estimation Algorithm with Gaussian Spin States. *PRX Quantum* **2021**, *2*, No. 040301.
(13) Peruzzo, A.; McClean, J.; Shadbolt, P.; Yung, M.-H.; Zhou, X.-Q.; Love, P. J.; Aspuru-Guzik, A.; O'Brien, J. L. A variational eigenvalue solver on a photonic quantum processor. *Nat. Commun.* **2014**, *5*, 4213.
(14) McClean, J. R.; Romero, J.; Babbush, R.; Aspuru-Guzik, A. The theory of variational hybrid quantum-classical algorithm. *New J. Phys.* **2016**, *18*, No. 023023.
(15) Romero, J.; Babbush, R.; McClean, J. R.; Hempel, C.; Love, P. J.; Aspuru-Guzik, A. Strategies for quantum computing molecular energies using the unitary coupled cluster ansatz. *Quantum Sci. Technol.* **2019**, *4*, No. 014008.
(16) Preskill, J. Quantum Computing in the NISQ era and beyond. *Quantum* **2018**, *2*, 79−99.
(17) McArdle, S.; Mayorov, A.; Shan, X.; Benjamin, S.; Yuan, X. Digital quantum simulation of molecular vibrations. *Chem. Sci.* **2019**, *10*, 5725−5735.
(18) Sparrow, C.; Martín-López, E.; Maraviglia, N.; Neville, A.; Harrold, C.; Carolan, J.; Joglekar, Y. N.; Hashimoto, T.; Matsuda, N.; O'Brien, J. L.; et al. Simulating the vibrational quantum dynamics of molecules using photonics. *Nature* **2018**, *557*, 660−667.
(19) Sawaya, N. P. D.; Huh, J. Quantum Algorithm for Calculating Molecular Vibronic Spectra. *J. Phys. Chem. Lett.* **2019**, *10*, 3586−3591.
(20) Johnson, M. W.; Amin, M. H. S.; Gildert, S.; Lanting, T.; Hamze, F.; Dickson, N.; Harris, R.; Berkley, A. J.; Johansson, J.; Bunyk, P.; et al. Quantum annealing with manufactured spins. *Nature* **2011**, *473*, 194−198.
(21) Teplukhin, A.; Kendrick, B. K.; Babikov, D. Calculation of Molecular Vibrational Spectra on a Quantum Annealer. *J. Chem. Theory Comput.* **2019**, *15*, 4555−4563.
(22) Teplukhin, A.; Kendrick, B. K.; Mniszewski, S. M.; Zhang, Y.; Kumar, A.; Negre, C. F. A.; Anisimov, P. M.; Tretiak, S.; Dub, P. A. Computing molecular excited states on a D-Wave quantum annealer. *Sci. Rep.* **2021**, *11*, 18796.
(23) Asnaashari, K.; Krems, R. Compact quantum circuits for variational calculations of ro-vibrational energy levels of molecules on a quantum computer. *arXiv:2303.09822*
(24) Althorpe, S. C.; Clary, D. C. Quantum Scattering Calculations on Chemical Reactions. *Annu. Rev. Phys. Chem.* **2003**, *54*, 493−529.
(25) Clary, D. C. Quantum Dynamics of Chemical Reactions. *Science* **2008**, *321*, 789.
(26) Zhang, D. H.; Guo, H. Recent Advances in Quantum Dynamics of Bimolecular Reactions. *Annu. Rev. Phys. Chem.* **2016**, *67*, 135−158.
(27) Kaiser, R. I.; Mebel, A. M. The reactivity of ground-state carbon atoms with unsaturated hydrocarbons in combustion flames and in the interstellar medium. *Int. Rev. Phys. Chem.* **2002**, *21*, 307−356.
(28) Herbst, E.; Yates, J. T. Introduction: Astrochemistry. *Chem. Rev.* **2013**, *113*, 8707−8709.
(29) Jasper, A. W.; Pelzer, K. M.; Miller, J. A.; Kamarchik, E.; Harding, L. B.; Klippenstein, S. J. Predictive a priori pressure-dependent kinetics. *Science* **2014**, *346*, 1212−1215.
(30) Klippenstein, S. J. From theoretical reaction dynamics to chemical modeling of combustion. *Proc. Combust. Inst.* **2017**, *36*, 77−111.
(31) Flynn, G. W.; Parmenter, C. S.; Wodtke, A. M. Vibrational Energy Transfer. *J. Phys. Chem.* **1996**, *100*, 12817−12838.
(32) Liu, K. Vibrational Control of Bimolecular Reactions with Methane by Mode, Bond, and Stereo Selectivity. *Annu. Rev. Phys. Chem.* **2016**, *67*, 91−111.
(33) Yang, D.; Huang, J.; Hu, X.; Guo, H.; Xie, D. Breakdown of energy transfer gap laws revealed by full-dimensional quantum scattering between HF molecules. *Nat. Commun.* **2019**, *10*, 4658.
(34) Kim, J. B.; Weichman, M. L.; Sjolander, T. F.; Neumark, D. M.; Kłos, J.; Alexander, M. H.; Manolopoulos, D. E. Spectroscopic observation of resonances in the F + H_2 →HF + H reaction. *Science* **2015**, *349*, 510.
(35) Wang, T.; Chen, J.; Yang, T.; Xiao, C.; Sun, Z.; Huang, L.; Dai, D.; Yang, X.; Zhang, D. H. Dynamical Resonances Accessible Only by Reagent Vibrational Excitation in the F + HD →HF + D Reaction. *Science* **2013**, *342*, 1499.
(36) Perreault, W. E.; Mukherjee, N.; Zare, R. N. Quantum control of molecular collisions at 1 Kelvin. *Science* **2017**, *358*, 356.
(37) Vogels, S. N.; Onvlee, J.; Chefdeville, S.; van der Avoird, A.; Groenenboom, G. C.; van de Meerakker, S. Y. T. Imaging resonances in low-energy NO-He inelastic collisions. *Science* **2015**, *350*, 787.
(38) Krems, R. V. Cold Controlled Chemistry. *Phys. Chem. Chem. Phys.* **2008**, *10*, 4079−4092.
(39) Carr, L. D.; DeMille, D.; Krems, R. V.; Ye, J. Cold and ultracold molecules: science, technology and applications. *New J. Phys* **2009**, *11*, No. 055049.
(40) Balakrishnan, N. Perspective: Ultracold molecules and the dawn of cold controlled chemistry. *J. Chem. Phys.* **2016**, *145*, 150901.
(41) Bohn, J. L.; Rey, A. M.; Ye, J. Cold molecules: Progress in quantum engineering of chemistry and quantum matter. *Science* **2017**, *357*, 1002−1010.
(42) Devolder, A.; Brumer, P.; Tscherbul, T. V. Complete Quantum Coherent Control of Ultracold Molecular Collisions. *Phys. Rev. Lett.* **2021**, *126*, 153403.
(43) Devolder, A.; Tscherbul, T. V.; Brumer, P. Coherent Control of Ultracold Molecular Collisions: The Role of Resonances. *J. Phys. Chem. Lett.* **2023**, *14*, 2171−2177.
(44) Nyman, G.; Yu, H.-G. Quantum theory of bimolecular chemical reactions. *Rep. Prog. Phys.* **2000**, *63*, 1001.
(45) Kassal, I.; Jordan, S. P.; Love, P. J.; Mohseni, M.; Aspuru-Guzik, A. Polynomial-time quantum algorithm for the simulation of chemical dynamics. *Proc. Natl. Acad. Sci. USA* **2008**, *105*, 18681−18686.
(46) Kassal, I.; Whitfield, J. D.; Perdomo-Ortiz, A.; Yung, M.-H.; Aspuru-Guzik, A. Simulating Chemistry Using Quantum Computers. *Annu. Rev. Phys. Chem.* **2011**, *62*, 185−207.
(47) Bian, T.; Kais, S. Quantum computing for atomic and molecular resonances. *J. Chem. Phys.* **2021**, *154*, 194107.
(48) Roggero, A.; Carlson, J. Dynamic linear response quantum algorithm. *Phys. Rev. C* **2019**, *100*, No. 034610.
(49) Du, W.; Vary, J. P.; Zhao, X.; Zuo, W. Quantum simulation of nuclear inelastic scattering. *Phys. Rev. A* **2021**, *104*, No. 012611.
(50) Lee, C.-K.; Hsieh, C.-Y.; Zhang, S.; Shi, L. Variational Quantum Simulation of Chemical Dynamics with Quantum Computers. *J. Chem. Theory Comput.* **2022**, *18*, 2105−2113.
(51) Zhang, J. Z. H.; Miller, W. H. Quantum reactive scattering via the S-matrix version of the Kohn variational principle: Integral cross sections for H + H_2 (v_1 = j_1 = 0) →H_2 (v_2 = 1, j_2 = 1,3) + H in the energy range *E*total = 0.9 − 1.4eV. *Chem. Phys. Lett.* **1988**, *153*, 465−470.
(52) Zhang, J. Z. H.; Miller, W. H. Quantum reactive scattering via the S-matrix version of the Kohn variational principle: Differential and integral cross sections for D + H_2 →HD + H. *J. Chem. Phys.* **1989**, *91*, 1528−1547.
(53) Bravo-Prieto, C.; LaRose, R.; Cerezo, M.; Subasi, Y.; Cincio, L.; Coles, P. J. Variational Quantum Linear Solver. *arXiv:1909.05820*

https://doi.org/10.1021/acs.jpclett.3c00985
J. Phys. Chem. Lett. 2023, 14, 6224−6233

(54) Zhang, J. Z. H.; Chu, S.; Miller, W. H. Quantum scattering via the S-matrix version of the Kohn variational principle. *J. Chem. Phys.* **1988**, *88*, 6233−6239.
(55) Ryabinkin, I. G.; Yen, T.-C.; Genin, S. N.; Izmaylov, A. F. Qubit Coupled Cluster Method: A Systematic Approach to Quantum Chemistry on a Quantum Computer. *J. Chem. Theory Comput.* **2018**, *14*, 6317−6326.
(56) Anand, A.; Schleich, P.; Alperin-Lea, S.; Jensen, P. W. K.; Sim, S.; Díaz-Tinoco, M.; Kottmann, J. S.; Degroote, M.; Izmaylov, A. F.; Aspuru-Guzik, A. A quantum computing view on unitary coupled cluster theory. *Chem. Soc. Rev.* **2022**, *51*, 1659−1684.
(57) Grimsley, H. R.; Economou, S. E.; Barnes, E.; Mayhall, N. J. An adaptive variational algorithm for exact molecular simulations on a quantum computer. *Nat. Commun.* **2019**, *10*, 3007.
(58) Kandala, A.; Mezzacapo, A.; Temme, K.; Takita, M.; Brink, M.; Chow, J. M.; Gambetta, J. M. Hardware-efficient variational quantum eigensolver for small molecules and quantum magnets. *Nature* **2017**, *549*, 242−246.
(59) Johnson, B. R. The multichannel Lod-Derivative Method for Scattering Calculations. *J. Comput. Phys.* **1973**, *13*, 445.
(60) Secrest, D.; Johnson, B. R. Exact Quantum-Mechanical Calculation of a Collinear Collision of a Particle with a Harmonic Oscillator. *J. Chem. Phys.* **1966**, *45*, 4556−4570.
(61) Stechel, E. B.; Walker, R. B.; Light, J. C. R-matrix solution of coupled equations for inelastic scattering. *J. Chem. Phys.* **1978**, *69*, 3518−3531.
(62) Manolopoulos, D. E.; Gray, S. K. Symplectic integrators for the multichannel Schrödinger equation. *J. Chem. Phys.* **1995**, *102*, 9214−9227.
(63) Ruf, B. A.; Miller, W. H. A new (Cartesian) reaction-path model for dynamics in polyatomic systems, with application to H-atom transfer in malonaldehyde. *J. Chem. Soc., Faraday Trans.* **1988**, *84*, 1523−1534.
(64) Petković, M.; Kühn, O. Multidimensional Hydrogen Bond Dynamics in Salicylaldimine: Coherent Nuclear Wave Packet Motion versus Intramolecular Vibrational Energy Redistribution. *J. Phys. Chem. A* **2003**, *107*, 8458−8466.
(65) Giese, K.; Kühn, O. The all-Cartesian reaction plane Hamiltonian: Formulation and application to the H-atom transfer in tropolone. *J. Chem. Phys.* **2005**, *123*, No. 054315.
(66) Giese, K.; Ushiyama, H.; Takatsuka, K.; Kühn, O. Dynamical hydrogen atom tunneling in dichlorotropolone: A combined quantum, semiclassical, and classical study. *J. Chem. Phys.* **2005**, *122*, 124307.
(67) Miller, W. H.; Handy, N. C.; Adams, J. E. Reaction path Hamiltonian for polyatomic molecules. *J. Chem. Phys.* **1980**, *72*, 99−112.
(68) Patterson, D.; Tsikata, E.; Doyle, J. M. Cooling and collisions of large gas phase molecules. *Phys. Chem. Chem. Phys.* **2010**, *12*, 9736.
(69) Li, Z.; Heller, E. J. Cold collisions of complex polyatomic molecules. *J. Chem. Phys.* **2012**, *136*, No. 054306.
(70) Piskorski, J.; Patterson, D.; Eibenberger, S.; Doyle, J. M. Cooling, Spectroscopy and Non-Sticking of trans-Stilbene and Nile Red. *ChemPhysChem* **2014**, *15*, 3800−3804.
(71) Möttönen, M.; Vartiainen, J. J.; Bergholm, V.; Salomaa, M. M. Transformation of Quantum States Using Uniformly Controlled Rotations. *Quantum Info. Comput.* **2005**, *5*, 467−473.
(72) Araujo, I. F.; Park, D. K.; Petruccione, F.; da Silva, A. J. A divide-and-conquer algorithm for quantum state preparation. *Sci. Rep.* **2021**, *11*, 6329.
(73) Volya, D.; Mishra, P. State Preparation on Quantum Computers via Quantum Steering. *arXiv:2302.13518*
(74) Wen, J.; Kong, X.; Wei, S.; Wang, B.; Xin, T.; Long, G. Experimental realization of quantum algorithms for a linear system inspired by adiabatic quantum computing. *Phys. Rev. A* **2019**, *99*, No. 012320.

https://doi.org/10.1021/acs.jpclett.3c00985
J. Phys. Chem. Lett. 2023, 14, 6224−6233